Volume 71, Number 19
October 1, 2007

ELSEVIER

Geochimica et Cosmochimica Acta

JOURNAL OF THE GEOCHEMICAL SOCIETY
AND THE METEORITICAL SOCIETY

Volume 71, Number 19 October 1, 2007

Articles

Continued on outside back cover

Available online at www.sciencedirect.com
ScienceDirect
Geochimica et Cosmochimica Acta 71 (2007) 4644–4654
Geochimica et Cosmochimica Acta
www.elsevier.com/locate/gca

The effect of U(VI) bioreduction kinetics on subsequent reoxidation of biogenic U(IV)

John M. Senko [a], Shelly D. Kelly [b], Alice C. Dohnalkova [c], Jeffrey T. McDonough [a], Kenneth M. Kemner [b], William D. Burgos [a,*]

[a] *Department of Civil and Environmental Engineering, The Pennsylvania State University, 212 Sackett Building, University Park, PA 16802, USA*
[b] *Advanced Photon Source, Argonne National Laboratory, Argonne, IL, USA*
[c] *Environmental Molecular Sciences Laboratory, Pacific Northwest National Laboratory, Richland, WA, USA*

Received 12 March 2007; accepted in revised form 23 July 2007; available online 26 August 2007

Abstract

Microbially mediated in situ reduction of soluble U(VI) to insoluble U(IV) (as UO_2) has been proposed as a means of preventing the migration of that radionuclide with groundwater, but preventing the oxidative resolubilization of U has proven difficult. We hypothesized that relatively slow rates of U(VI) bioreduction would yield larger UO_2 precipitates that would be more resistant to oxidation than those produced by rapid U(VI) bioreduction. We manipulated U(VI) bioreduction rates by varying the density of *Shewanella putrefaciens* CN32 added to U(VI) containing solutions with lactate as an electron donor. Characterization of biogenic UO_2 particles by extended X-ray absorption fine-structure spectroscopy and transmission electron microscopy revealed that UO_2 nanoparticles formed by relatively slow rates of U(VI) reduction were larger and more highly aggregated than those formed by relatively rapid U(VI) reduction. UO_2 particles formed at various rates were incubated under a variety of abiotically and biologically oxidizing conditions. In all cases, UO_2 that was formed by relatively slow U(VI) reduction was oxidized at a slower rate and to a lesser extent than UO_2 formed by relatively rapid U(VI) bioreduction, suggesting that the stability of UO_2 in situ may be enhanced by stimulation of relatively slow rates of U(VI) reduction.
Published by Elsevier Ltd.

1. INTRODUCTION

Uranium contaminates aquifers where that element was mined and processed for the production of weapons and fuel. Uranium is predominantly encountered in these aquifers in an oxidized (+VI) valence state, which is quite soluble and easily migrates with the groundwater, threatening nearby water supplies (Murphy and Shock, 1999). However, in a reduced valence state (+IV), uranium is quite insoluble, so the reduction of soluble U(VI) to insoluble U(IV) (as uraninite) is a reaction that may be exploited to prevent the migration of U with groundwater (Murphy and Shock, 1999). Most naturally occurring uraninite contains U(VI) "defects" and is most precisely identified by the formula UO_{2+x} (where $0 \leqslant x \leqslant 0.25$) (Burns, 1999), but for simplicity will be identified as UO_2. Anaerobic microbiological activity may lead to U(VI) reduction via the reaction of that element with products of anaerobic respiration (Fe(II) or sulfide) or by enzymatic U(VI) reduction, coupled with oxidation of organic carbon or H_2 (Lovley et al., 1991; Gorby and Lovley, 1992; Wersin et al., 1994; Liger et al., 1999). Therefore, a strategy for stimulating bacterially mediated U(VI) reduction is to inject a physiological electron donor into a U(VI) contaminated aquifer that will bring about anoxic conditions, and consequently, stimulate U(VI) reducing bacterial activity (Anderson et al., 2003; Istok et al., 2004).

Unfortunately, the stability of U(IV) once it is immobilized in an aquifer is difficult to predict. Recent work has illustrated the susceptibility of biogenic U(IV) to chemical

* Corresponding author. Fax: +1 814 863 7304.
E-mail address: wdb3@psu.edu (W.D. Burgos).

0016-7037/$ - see front matter Published by Elsevier Ltd.
doi:10.1016/j.gca.2007.07.021

oxidation by O_2 (Abdelouas et al., 1999; Duff et al., 1999), nitrite (Senko et al., 2002; Senko et al., 2005b), and Fe(III) (hydr)oxides (Nevin and Lovley, 2000; Senko et al., 2005b; Ginder-Vogel et al., 2006), and to biological oxidation coupled with O_2 (DiSpirito and Tuovinen, 1982) or nitrate (Finneran et al., 2002; Beller, 2005) reduction. Consequently, strategies for reductive immobilization of U must include considerations for preventing or minimizing its oxidative remobilization.

The rate of mineral formation (whether biologically catalyzed or abiotic) can control the physical properties of those minerals. For instance, rapidly formed minerals may be less crystalline and/or smaller than their relatively slowly formed counterparts (Cornell and Schwertmann, 2003; Fredrickson et al., 2003; Glasauer et al., 2003; van der Zee et al., 2003; Han et al., 2005; Senko et al., 2005a), and these differences in physical characteristics may have a profound effect on their reactivity (Lovley and Phillips, 1987; Deng and Stumm, 1994; Zachara et al., 1998; Glasauer et al., 2003; Roden, 2003; Hansel et al., 2004). In light of this observation, we hypothesized that relatively slow rates of U(VI) bioreduction would give rise to larger and less reactive U(IV) phases that would be more resistant to oxidation than relatively rapidly formed biogenic U(IV) phases.

To assess the effect of U(VI) bioreduction kinetics on the characteristics of resultant U(IV) precipitates, we manipulated rates of U(VI) reduction by varying the density of the U(VI)-reducing bacterium *Shewanella putrefaciens* CN32 in U(VI) reduction incubations. Biogenic U(IV) precipitates formed at different rates were characterized by extended X-ray absorption fine-structure spectroscopy (EXAFS) and transmission electron microscopy (TEM). To assess the redox stability of UO_2 particles produced at various rates, we tested the susceptibility of these particles to oxidation by O_2, nitrite, nitrite with Fe as an electron shuttle, Fe(III) (hydr)oxide, and *Thiobacillus denitrificans* with nitrate as an electron acceptor.

2. MATERIALS AND METHODS

2.1. Cell cultivation and incubation

Shewanella putrefaciens CN32 was grown aerobically on tryptic soy broth (TSB) without dextrose to late log phase and harvested by centrifugation (Burgos et al., 2007). Cells were resuspended and washed three times in anoxic bicarbonate buffer (30 mM, pH 6.8) before resuspension in the same buffer. The cell suspension, containing approximately 1.1×10^{10} cell/ml, was used to inoculate anoxic U(VI) bioreduction medium containing 5 mM sodium lactate, 1.4 mM uranyl acetate, and 30 mM sodium bicarbonate (pH 6.8, under 80:20% N_2:CO_2 atm) (Balch et al., 1979). To manipulate the rates of U(VI) reduction, 10, 4, or 1 ml of cell suspension was added to separate U(VI) bioreduction medium-containing (500 ml) bottles to achieve cell densities of approximately 2.2×10^8 cell/ml, 9.1×10^7, and 2.3×10^7 cell/ml, respectively. Incubations were maintained at 23 °C in darkness. Samples were periodically removed and soluble U(VI) in the incubations was quantified as described below.

Thiobacillus denitrificans (ATCC 25259) was grown in medium described by Beller (2005), which contained 18 mM NH_4Cl, 14.7 mM KH_2PO_4, 3.25 mM $MgSO_4$, 0.08 mM $FeSO_4$, 0.05 mM $CaCl_2$, and vitamins and trace metals as described by Tanner (1997). The medium was prepared anoxically, buffered with 30 mM $NaHCO_3$ (pH 6.8, under 80:20% N_2:CO_2 atm) and contained thiosulfate (20 mM NaS_2O_3) as the sole electron donor with nitrate (20 mM KNO_3) as the sole terminal electron acceptor. Cells were grown to late log phase, harvested, and washed as described above. Cells in suspension were enumerated by acridine orange direct cell counts (AODC) (Parsons et al., 1984) and added to the incubations described below to achieve a cell density of approximately 1×10^8 cell/ml.

2.2. U(IV) oxidation experiments

All biogenic U(IV) oxidation experiments were conducted in 30 mM $NaHCO_3$-buffered solution (pH 6.8, under 80:20% N_2:CO_2 atm). Upon complete U(VI) reduction in the all of the incubations described above (i.e., after U(VI) reduction in the incubation containing the lowest cell density), cell/U(IV)-containing suspensions were pasteurized at 70 °C for 5 min to deactivate biological activity. To determine if cells were deactivated, a pasteurized cell suspension was transferred to TSB. No growth was observed in pasteurized cell-inoculated TSB, assuring us that cells were deactivated. Biogenic U(IV) was added to bicarbonate buffered medium to achieve a U(IV) concentration of approximately 100 μM. A uniform cell density in all U(IV) oxidizing incubations was achieved by adding pasteurized U-free *S. putrefaciens* CN32, where necessary, to achieve a final inactivated cell concentration of approximately 2.2×10^7 cell/ml.

Oxygen was provided to incubations by flushing the headspace of anoxic bicarbonate buffer-containing bottles with filter-sterilized air. To maintain the pH of the bicarbonate buffered medium, 20% of the air headspace was removed and replaced with an equivalent volume of CO_2. No change in medium pH resulted from these manipulations. Hydrous ferric oxide (HFO) was prepared as described by Lovley and Phillips (1987) and Schwertmann and Cornell (1991), bubbled for 1 h with oxygen-free N_2, and pasteurized. Fe(III) (HFO; initial concentration 5 mM), nitrite ($NaNO_2$; initial concentration 5 mM), nitrate ($NaNO_3$; initial concentration 5 mM), and Fe(II) ($FeCl_2$; initial concentration 50 μM) were added to bicarbonate-buffered medium from anoxic stock solutions/suspensions. For incubations containing *T. denitrificans*, 3% H_2 was included in the headspace of bottles (Beller, 2005).

2.3. Analytical techniques

Total U(VI) (including soluble and solids-associated U(VI)) and total U (including U(VI) and U(IV)) were measured as described by Elias et al. (2003). Briefly, samples were removed from incubations by syringe in an anoxic glovebag (95:5% N_2:H_2 atm; Coy Laboratory Products Inc.; Grass Lake, MI) and placed in an equivalent volume of 1 M anoxic $NaHCO_3$ (pH 8.4). After extraction for

5 min, solids were removed by centrifugation and total U(VI) in the supernatant was measured as described below. To measure total U, samples were placed in oxic 10% HNO_3 under air to oxidize all U(IV). U(VI) was measured by kinetic phosphorescence analysis on a KPA-11 (Chem-Chek Instruments, Richland, WA) (Brina and Miller, 1992).

2.4. X-ray absorption spectroscopy

Precipitates were analyzed by U L_{III}-edge X-ray absorption spectroscopy (XAS) at the Materials Research Collaborative Access Team (MR-CAT) sector 10-ID beamline (Segre et al., 2000) of the Advanced Photon Source (APS) at Argonne National Laboratory (ANL). The XAS spectra were collected in transmission mode using quick-scanning of the monochromator. MR-CAT beamline set-up details are described by O'Loughlin et al. (2003).

Upon removal of $\geqslant$95% of U(VI) from solution (putatively identified as reduction of U(VI) to U(IV)) by *S. putrefaciens*, cell-U(IV) suspensions were concentrated by centrifugation and stored at 4 °C before shipment to ANL. Samples (approximately 40 mg cell-U(IV) paste) were mounted in holes machined in Plexiglas sample holders and covered with Kapton film and sealed with Kapton tape. All sample preparation was performed in a Coy anoxic glovebag and all samples were stored in the chamber prior to analysis. Samples mounted in the holders were exposed to the atmosphere for less than 1 min before being mounted for XAS measurements in a free-flowing N_2 environment to limit possible sample oxidation. Previous investigations of these XAS sample holders demonstrated that they maintained anoxic integrity more than 8 h.

To determine the average valence state within the samples the X-ray absorption edge energy was monitored by collecting the reference spectrum from hydrogen uranyl phosphate (U(VI) Std) during the collection of each spectrum for energy calibration. An abiotic nanoparticulate UO_2 standard (U(IV) Std) (O'Loughlin et al., 2003) was also measured for X-ray absorption near edge structure (XANES) comparisons. All data sets were accurately aligned in energy using the derivative of the edge of the U(VI) standard. Uranium XANES spectra were collected in 30 s intervals consecutively for 5 min to monitor the spectra for radiation-induced changes to the samples. No changes were detected on the 30 s time scale. The extended X-ray absorption fine structure (EXAFS) spectra were collected at different sample locations with the X-ray exposure of less than 5 min at each region. The EXAFS spectra were averaged and then the background was removed using the programs Athena (Ravel and Newville, 2005) and IFEFFIT (Newville, 2001). The background removal parameter Rbkg was set to 1.0 Å (Newville et al., 1993). The EXAFS spectra were modeled using theoretical models from the atomic clusters of uraninite (Wyckoff, 1960) and autunite (Locock and Burns, 2003) as input for FEFF 7.02 (Zabinski et al., 1995). The EXAFS parameters were optimized to the measured spectra using the program FEFFIT (Stern et al., 1995). The U EXAFS signal is due to the coordination of atoms within a shell at a given distance from the uranium atoms. The EXAFS parameters are the amplitude reduction factor (S_0^2), an energy shift to align the theoretical and measured spectra (ΔE_0), the number of atoms within a shell or coordination number (CN), distance between the uranium atom and the neighboring atoms (R), and the mean square displacement in that distance (σ^2). Details of the EXAFS model are given in the electronic annex EA-1.

2.5. Transmission electron microscopy

To maintain the redox state of the newly formed U material, all sample preparation for transmission electron microscopy (TEM) was performed in a Coy anoxic glovebag. Upon removal of $\geqslant$95% of U(VI) from solution, cell-UO_2 suspensions were fixed with 2% anoxic glutaraldehyde, washed, and gradually dehydrated in an ethanol series. Material was infiltrated in LR White resin and embedded at 60 °C overnight. Polymerized blocks were sectioned on an ultramicrotome (Leica UCT, Wetzlar, Germany) into 70 nm thin sections and mounted on copper grids that were coated with formvar and carbon. Unstained cells and UO_2 particles were visualized on a JEOL 2010 TEM operated at 200 kV. Images were collected digitally using a Gatan 1 K Multiscan CCD camera and analyzed using Digital Micrograph software (Gatan Inc., Pleasanton, CA).

3. RESULTS

3.1. U(VI) bioreduction

The rate of U(VI) bioreduction was likely dependent on a number of factors, including the concentrations of cells, dissolved U(VI) and lactate, temperature, mixing conditions, and possibly, the concentration ratios of U(VI)/cell, lactate/cell, and U(VI)/lactate. A mathematical expression for the rate of U(VI) bioreduction could be posited to include a term for all of these factors (e.g., as in multi-Monod kinetics). However, we found that the reaction was zero-order with respect to total U(VI) and zero-order with respect to lactate, and therefore, we have used the following equation to model the rate of U(VI) bioreduction:

$$R = \mathrm{d}[\mathrm{U(VI)}]/\mathrm{d}t = -k[\mathrm{DMRB}] \quad (1)$$

where R is the rate of total U(VI) as a function of time (μmol U(VI) l^{-1} d^{-1}). k is a zero-order cell dependent rate constant (μmol l^{-1} d^{-1} (cell/ml)$^{-1}$). [DMRB] is the initial density of *S. putrefaciens* CN32 (cell/ml), and [U(VI)] is the total U(VI) concentration (μmol U(VI) l^{-1}).

To produce U(IV) at different rates, we incubated *S. putrefaciens* CN32 with U(VI) at cell densities of 2.2×10^8 cell/ml, 9.1×10^7, and 2.3×10^7 cell/ml to yield zero order U(VI) bioreduction rates of 602 μM/d (designated $U(IV)_{fast}$), 182 μM/d ($U(IV)_{med}$), and 55 μM/d ($U(IV)_{slow}$), respectively (Fig. 1). The initial cell-normalized U(VI) reduction rate in these three incubations was 236 ± 33 μM/d/10^8 cell (mean ± s.d.). Using a Michaelis–Menten model of U(VI) reduction by *S. putrefaciens* CN32 under identical conditions with previously reported data (Burgos et al., 2007), we calculated a V_{max} of

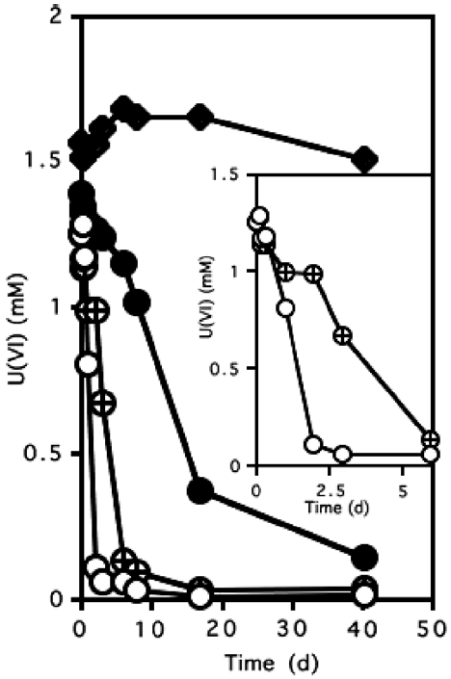

Fig. 1. U(VI) reduction by (♦) 0, (○) 2.2×10^8, (⊕) 9.1×10^7, and (●) 2.3×10^7 cell/ml *S. putrefaciens* CN32. U(IV) products of U(VI) reduction by 2.2×10^8 cell/ml, 9.1×10^7 cell/ml, and 2.3×10^7 cell/ml were designated $U(IV)_{fast}$, $U(IV)_{med}$, and $U(IV)_{slow}$, respectively. The inset shows U(VI) concentrations in the first 6 d of $U(IV)_{fast}$ and $U(IV)_{med}$ incubations.

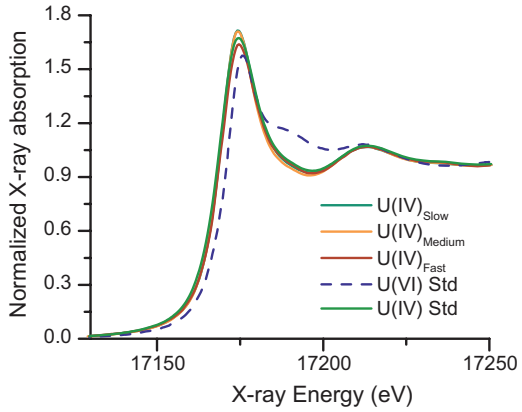

Fig. 2. Normalized X-ray absorption near-edge spectra (XANES) of solid phase U formed in $U(IV)_{fast}$, $U(IV)_{med}$, and $U(IV)_{slow}$ incubations of *S. putrefaciens* CN32 with U(VI) and lactate. Spectra of abiotic nanoparticulate uraninite ($U(IV)_{std}$) and hydrogen uranyl phosphate ($U(VI)_{std}$) standards are also provided.

220 μM/d/10^8 cell and K_m of 45 μM. The rates of U(VI) reduction observed in the present study are consistent with the V_{max} of our previous experiments, and suggest that a zero-order model is appropriate for the majority of U(VI) reduction in these experiments (i.e., the U(VI) reducing enzyme(s) were saturated through much of the U(VI) reducing incubations). We observed negligible loss of U(VI) from solution in incubations that contained cells, were aerated, and did not contain lactate (data not shown), suggesting that U(VI) precipitation in anoxic, lactate-containing incubations was due to U(VI) reduction and not due to sorption to cells.

3.2. Characterization of U(IV) precipitates

Upon near-complete removal of U(VI) from solution, we noted differences in the shade of precipitates formed in U(VI) reducing incubations, with $U(IV)_{fast}$ incubations appearing brown, $U(IV)_{med}$ incubations a slightly darker brown, and $U(IV)_{slow}$ incubations appearing black. The formation of dark precipitates is consistent with the bioreduction of U(VI) to U(IV) (Gorby and Lovley, 1992). The X-ray absorption near edge structures for biogenic U precipitates closely matched that of a U(IV) standard of abiotic UO_2 nanoparticles, suggesting that the majority of biogenic U precipitates were in the +IV valence state (likely as UO_2) (Fig. 2). UO_2 particles were characterized by EXAFS to determine speciation of U(IV). Similar to previous studies (Suzuki et al., 2002; O'Loughlin et al., 2003) the decrease in the amplitude of the second peak (~3.7 Å) in the magnitude of the Fourier transform of EXAFS data with increasing reduction rate suggests that UO_2 particles formed in $U(IV)_{slow}$ incubations were larger than those in $U(IV)_{med}$ incubations, which were larger than particles present in $U(IV)_{fast}$ incubations (Fig. 3). The EXAFS spectra were modeled with two O shells (O1 and O2), a P shell, and a U shell. The bond lengths were determined to be 2.28 ± 0.01 Å for the U–O1 shell, 2.44 ± 0.01 Å for the U–O2 shell, 3.66 ± 0.02 Å for the U–P shell, and 3.85 ± 0.01 Å for the U–U shell (see electronic annex EA-1 for details).

The U–P distance of 3.66 ± 0.02 Å is typical for a monodentate bond between a P-containing ligand and the uranium atom (sharing one oxygen atom) (Morosin, 1978; Locock and Burns, 2003). The source of the phosphorous in the outer coordination shell of the uranium in these precipitates remains unclear. A similar distance has been previously reported for U(VI) bound to biomass (Kelly et al., 2002; Francis et al., 2004). The trend in the U–P coordination number with increased reduction rates shows the amount of phosphorous bound to the uranium decreases as the particles become larger. This trend is consistent with a biomass origin of the phosphoryl-ligand, since samples with larger UO_2 particles would have a smaller percentage of the surface associated U atoms of the particles available for interaction with the phosphoryl groups. However, it does not rule out the possibility that the source of the U–P interactions is a result of free phosphate carried with cells from the culture medium. The U–U distance of 3.85 ± 0.01 Å is consistent with the formation of nanoparticulate UO_2. Based on X-ray diffraction crystal structure, the U–U distance for large uraninite particles is 3.867 Å (Wyckoff, 1960). Previous EXAFS studies have shown that the U–U distance contracts from 3.86 to 3.87 Å in UO_2 particles larger than ~100 nm (O'Loughlin et al., 2003; Pierce et al., 2005) to 3.80–3.84 Å in UO_2 particles smaller than ~2 nm (Suzuki et al., 2002; O'Loughlin et al., 2003).

As mentioned above, further evidence of nanoparticulate UO_2 is in the decrease of the EXAFS U–U coordination

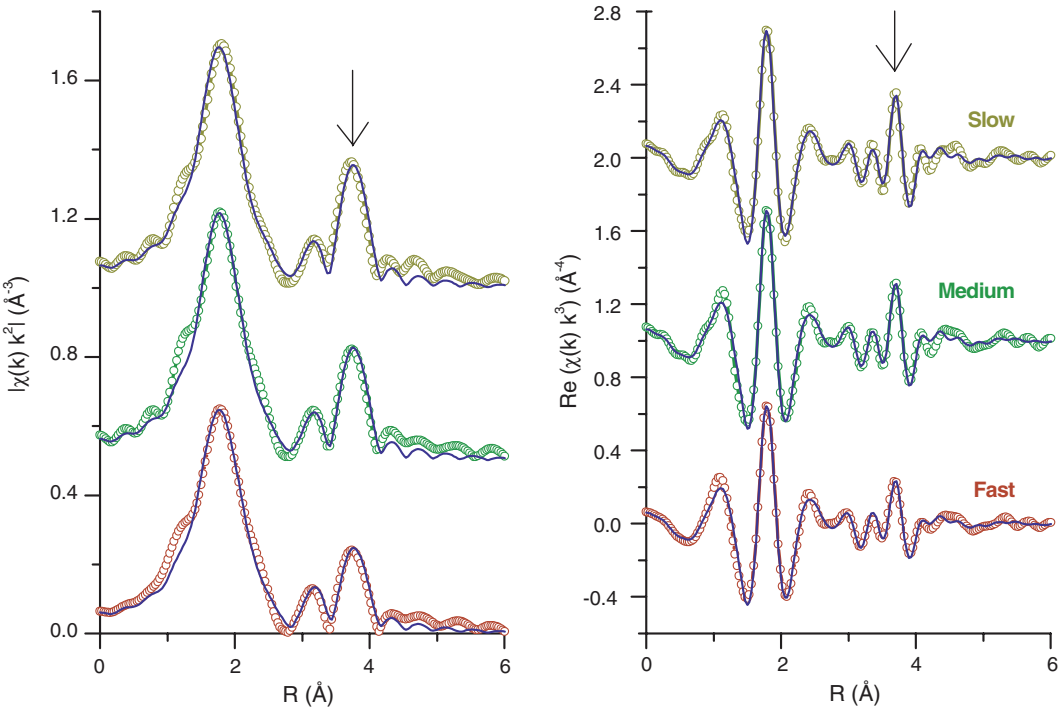

Fig. 3. Magnitude (left panel) and Real part (right panel) of the Fourier transform of EXAFS data (symbols) and model (lines) obtained from UO_2 particles in $U(IV)_{slow}$, $U(IV)_{med}$, and $U(IV)_{fast}$ incubations. The decrease in the height of the second peak (arrow) with increasing U(VI) reduction rate is suggestive of progressively smaller UO_2 particles produced by progressively greater rates of U(VI) reduction. EXAFS spectra were modeled with two O shells (O1 and O2), a P shell, and a U shell.

number from 12 for "bulk" UO_2 particles to 4.6 ± 1.0, 6.2 ± 0.8, and 6.8 ± 1.2 for the $U(IV)_{fast}$, $U(IV)_{med}$, and $U(IV)_{slow}$ precipitates, respectively. The EXAFS U–U coordination number is the average number of neighbors for all U atoms within the sample. The uranium atoms on the surface of a particle are under-coordinated and the number of the under-coordinated U atoms becomes significant for particle sizes less than 10 nm. In addition to under-coordinated surface atoms or the U–O–P interactions at the surfaces of uraninite nanoparticles, the U–P signal also indicates that UO_2 is not the only uranium species within the sample. For example, mono-dispersed uranium atoms bound to P-ligands would contribute to decreasing the U–U coordination number, since these atoms (if present) do not have a U neighbor. If we neglect the possibility of mono-dispersed U, the average UO_2 particle sizes are estimated to be approximately 1.4, 1.2, and 0.9 nm for $U(IV)_{slow}$, $U(IV)_{med}$, and $U(IV)_{fast}$, respectively. If we include the possibility of mono-dispersed U, the average estimated UO_2 particle sizes would increase. For example, if we assume a bi-modal distribution of 25% monomeric uranium bound to phosphoryl-ligands and 75% uranium within UO_2 particles, then the EXAFS U–U coordination number for the UO_2 would increase by 25% from 6.8 to 8.5 for the $U(IV)_{slow}$ precipitates, resulting in a larger estimated particle size of approximately 2 nm. For mixed systems, of mono-dispersed U and UO_2 particles, the trend in the EXAFS U–U coordination number indicates that the average particle size increased and/or the fraction of U atoms within the uraninite structure increased with decreasing bioreduction rate. The TEM results confirmed that the average particle size of uraninite increased with decreasing reduction rate.

Examination of *S. putrefaciens* CN32 cells and UO_2 particles from $U(IV)_{fast}$, $U(IV)_{med}$, and $U(IV)_{slow}$ incubations by TEM revealed variability in bacteria-mineral associations and aggregation state of UO_2 precipitates (Fig. 4). Direct measurement of UO_2 particle sizes in $U(IV)_{fast}$, $U(IV)_{med}$, and $U(IV)_{slow}$ incubations by TEM showed UO_2 particles in $U(IV)_{fast}$ incubations were approximately 2.5 nm in diameter (Fig. 4d), and particles in $U(IV)_{med}$ incubations were approximately 3 nm (Fig. 4e). UO_2 particles from $U(IV)_{slow}$ incubations of approximately 3 nm appeared to arrange themselves into larger, tightly-packed aggregates of 10 nm or more in diameter (Fig. 4f). UO_2 particles in $U(IV)_{fast}$ incubations were diffuse and associated almost exclusively with the periplasm of *S. putrefaciens* CN32 (Fig. 4a and d). UO_2 particles in $U(IV)_{med}$ incubations were deposited in both the periplasm and extracellularly (Fig. 4b and e). Periplasmic UO_2 particles in $U(IV)_{med}$ incubations were more densely packed than those in $U(IV)_{fast}$ incubations (Fig. 4d and e). UO_2 particles in $U(IV)_{slow}$ incubations were predominantly deposited extracellularly with very diffuse deposits in the periplasm (Fig. 4c and f). Extracellular UO_2 particles in $U(IV)_{slow}$ incubations appeared to originate as smaller particles that organized themselves into larger aggregates with aligned continuous d-lines (Fig. 4g–i) similar to those previously presented by Suzuki et al. (2002). In summary, larger, more highly aggregated UO_2 particles resulted from slower rates of U(VI) reduction. UO_2 that was produced at faster rates of U(VI) reduction

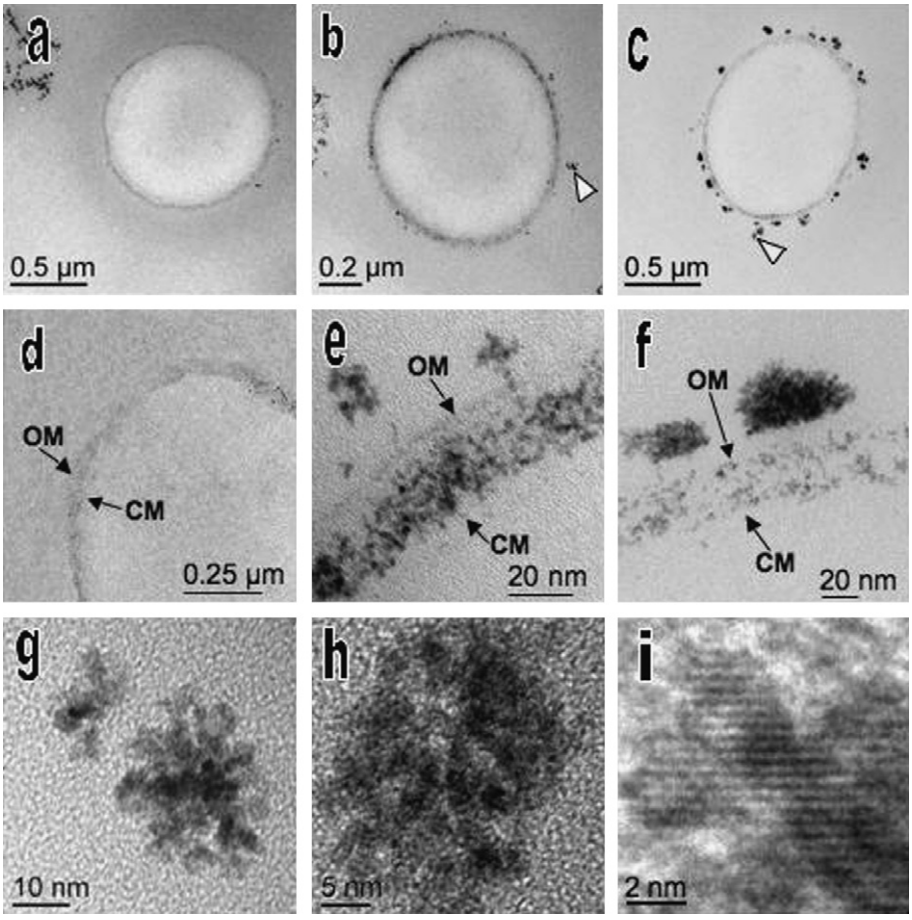

Fig. 4. Transmission electron micrographs of unstained *S. putrefaciens* CN32 cells and UO_2 precipitates after complete reduction of U(VI) in $U(IV)_{fast}$ (a and d), $U(IV)_{med}$ (b and e), and $U(IV)_{slow}$ (c, f–i) incubations. (a–c) Provide a view of an entire cell with UO_2 particles present in the periplasm or extracellularly (white arrows). (d–f) Provide a more detailed view of UO_2 particles in the periplasm of cells (OM, outer membrane; CM, cytoplasmic membrane). (g–i) Provide more detailed views of UO_2 aggregates present in $U(IV)_{slow}$ incubations, with aligned continuous d-lines present in the UO_2 particles (i).

was predominantly associated with the periplasm while UO_2 that was produced at slower rates of U(VI) reduction was deposited extracellularly.

3.3. Biological and abiotic oxidation of $U(IV)_{fast}$, $U(IV)_{med}$, and $U(IV)_{slow}$

UO_2 precipitates from $U(IV)_{fast}$, $U(IV)_{med}$, and $U(IV)_{slow}$ incubations were incubated with a variety of oxidants, including O_2 (in air) (Fig. 5a), *T. denitrificans* with nitrate as a terminal electron acceptor (Fig. 5b), Fe(III) (as hydrous ferric oxide) (Fig. 5c), nitrite with 50 μM Fe(II) provided as an electron shuttle (Fig. 5e), and nitrite alone (Fig. 5f). In all cases, UO_2 precipitates that were produced at a relatively faster rate were oxidized at a faster rate and to a greater extent than those that were formed at a relatively low rate (i.e., oxidation rate of $U(IV)_{fast} > U(IV)_{med} > U(IV)_{slow}$). No UO_2 oxidation was observed in the oxidant-free incubations (Fig. 5d). Incubation of UO_2 precipitates with air led to near-complete ($\geqslant 83\%$) oxidation of UO_2 within 6 h (Fig. 5a), and complete oxidation within 24 h. No other oxidant led to complete oxidation of UO_2, even after extended incubations of up to 480 h. UO_2 was not completely oxidized in incubations that contained nitrite as an oxidant with 50 μM Fe(II) as an electron shuttle (Fig. 5e). This type of incubation has been shown to completely oxidize U(IV) in previous studies (Senko et al., 2005b). When we incubated UO_2 particles from $U(IV)_{fast}$ incubations with nitrite alone (no Fe(II)), it was rapidly and extensively oxidized compared to UO_2 particles from $U(IV)_{med}$ and $U(IV)_{slow}$ incubations (Fig. 5f). Previous work has shown that in the absence of Fe(II) as an electron shuttle, nitrite is a relatively poor oxidant of U(IV) (Senko et al., 2005b).

4. DISCUSSION

4.1. Localization of UO_2 precipitates

Upon complete reduction of U(VI) by *S. putrefaciens* CN32, UO_2 particles were found in the periplasm or extracellularly in a fashion similar to previous studies (Fredrickson et al., 2002; Marshall et al., 2006). We observed differences in the cellular location of UO_2 precipitates in

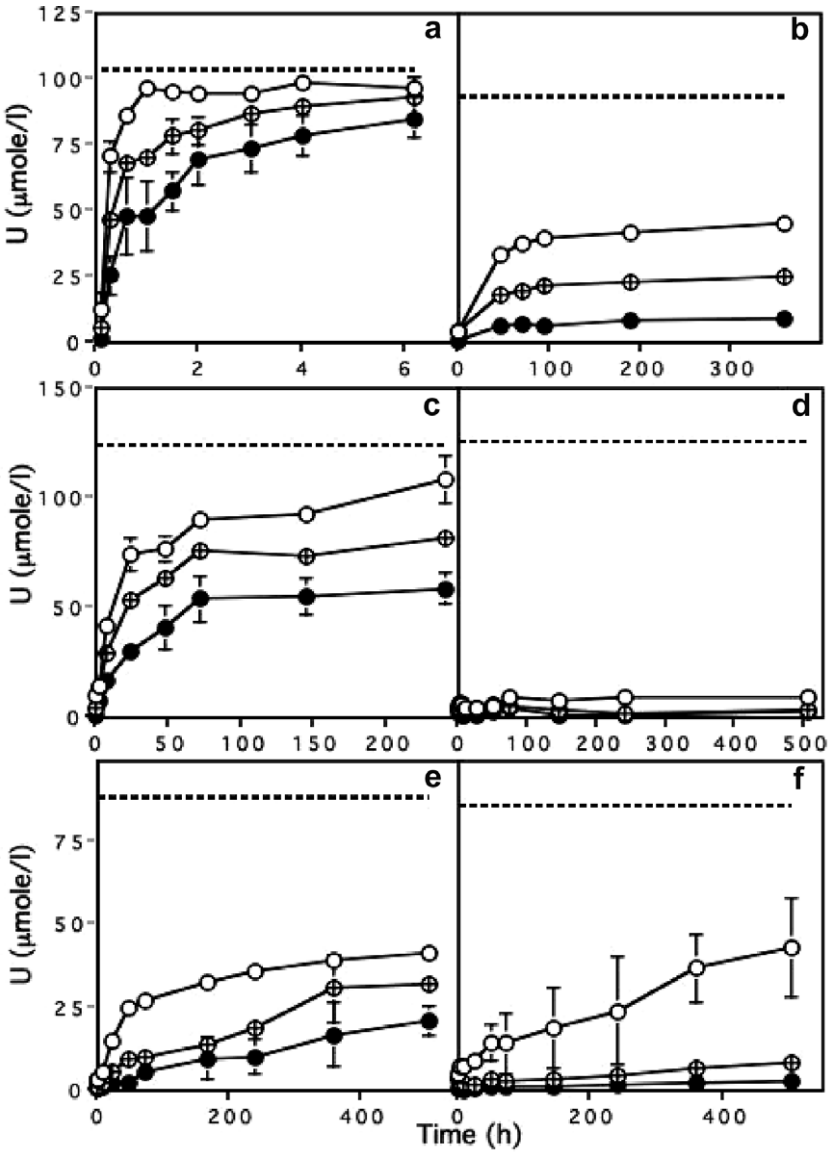

Fig. 5. U(VI) concentrations in incubations containing UO_2 particles from (○) $U(IV)_{fast}$, (⊕) $U(IV)_{med}$, and (●) $U(IV)_{slow}$ incubations with (a) O_2, (b) *T. denitrificans* with nitrate as the sole terminal electron acceptor, (c) hydrous ferric oxide (HFO), (d) no added oxidant, (e) nitrite with 50 μM Fe(II) as an electron shuttle, and (f) nitrite. The mean of the total U concentration (including U(VI) and U(IV)) in each incubation is represented by the dashed line. Error bars represent one standard deviation.

$U(IV)_{fast}$, $U(IV)_{med}$, and $U(IV)_{slow}$ incubations, with the general trend of more UO_2 in the periplasm in $U(IV)_{fast}$ incubations, and more UO_2 deposited extracellularly in $U(IV)_{slow}$ incubations. Cells with extensive deposits of extracellular UO_2 contained little periplasmic UO_2. We observed few cells that contained large amounts of both periplasmic UO_2 and extracellular UO_2. These results suggest that U(VI) may be reduced in the periplasm and exported out of the cell via active or passive processes. While our evidence for intracellular reduction and transport of UO_2 out of the cell is equivocal, we believe this activity could alleviate UO_2-product inhibition of U(VI) reduction, allowing further U(VI) reduction to proceed. Since U(VI) reduction rates were manipulated by varying the density of cells added to incubations, in incubations containing lower cell concentrations (e.g., $U(IV)_{slow}$), an individual cell would reduce more moles of U(VI) than one present in an incubation with a high cell density (e.g., $U(IV)_{fast}$). We emphasize that while overall rates of U(VI) reduction in the $U(IV)_{fast}$, $U(IV)_{med}$, and $U(IV)_{slow}$ incubations varied, the cell density-normalized rates were nearly identical.

We can not exclude the possibility of extracellular or membrane-bound, redox-active biomolecules (e.g., cytochromes) playing a role in extracellular UO_2 accumulation (Marshall et al., 2006). For instance, we have observed considerable differences in UO_2 location and characteristics between *Shewanella oneidensis* MR-1 cells grown on TSB (as we did here) and those grown under O_2-limited conditions in a chemically defined medium (Gorby et al., 2006; McDonough, 2006), and we have attributed these differ-

ences in cellular UO_2 location to differences in the amount of extracellular redox active proteins. Since we pasteurized cell-UO_2 suspensions before oxidation experiments, it is unlikely that cellular location of UO_2 particles alone exerted significant influence on the rate and extent of UO_2 oxidation. If cellular location of UO_2 particles did significantly influence the rate and extent of U(IV) oxidation, we would expect that extracellular UO_2 particles (such as those found predominantly in $U(IV)_{slow}$ incubations) would be more rapidly oxidized. This was not the case. Rather, the size of UO_2 particles strongly influenced their susceptibility to oxidation.

4.2. UO_2 particle size and aggregation

We observed U(VI) bioreduction rate-dependent trends in UO_2 particle size, where $U(IV)_{fast} < U(IV)_{med} < U(IV)_{slow}$ by particle size measurements using both TEM and EXAFS. While there were discrepancies in actual particle sizes determined by TEM and estimated by EXAFS (e.g., particle sizes of 3 and 2 nm, respectively, in $U(IV)_{slow}$ incubations), the trend of increasing particle size with decreasing reduction rate was still readily apparent. An explanation for this discrepancy is that the EXAFS-based measurement represents an average of the sizes of particles in the sample and includes monomeric U(IV) and particles too small to be visualized by TEM ($\leqslant$ approx. 1.5 nm), thus leading to smaller particle sizes as determined by EXAFS. Another explanation for the discrepancies in estimated UO_2 particle sizes is the presence of a phosphoryl-ligand associated U(IV) atoms, leading to a reduced estimation of UO_2 particle sizes determined by EXAFS. The amount of U(IV)-phosphoryl interactions detected by EXAFS decreased with decreasing reduction rate, suggesting that the phosphorous group arises from cell material or from free phosphate associated with cells. The large amount of extracellular UO_2 (that also contained less phosphorous) observed by TEM supports this hypothesis. While the presence of U(IV)-phosphoryl interactions has not been previously observed by EXAFS analysis of UO_2 particles, U(IV)–CO_2 or ─COOH and Fe (hydr)oxide interactions have been observed in biogenic and abiotic UO_2 particles (Suzuki et al., 2003; Boyanov et al., 2007), and P has been shown to be associated with UO_2 particles produced by *S. oneidensis* MR-1 (Marshall et al., 2006). Phosphoryl or phosphate groups have also been shown to be associated with Cr(III) produced by *Pseudomonas fluorescens* (Kemner et al., 2004). Potential roles of the U(IV)-P association that we show here are discussed in more detail below.

Both the particle size and aggregation state of biogenic UO_2 particles will likely influence their susceptibility to oxidation due to the lower surface area of larger or more highly aggregated particles. Enhanced reactivity of smaller UO_2 particles could simply be due to the greater exposed reactive surface area of smaller particles or the accumulation of insoluble U(VI) species on UO_2 grain boundaries that limit their further reaction with oxidants (Trocellier et al., 1995; Wronkiewicz et al., 1997; Casas et al., 1998). The role of U(IV)-associated phosphoryl groups (observed by EXAFS) in the oxidation of biogenic U(IV) is unclear. However, since we observed a direct correlation between the abundance of phosphoryl groups and the rate and extent of U(IV) oxidation, it is possible that phosphoryl groups may enhance surface reactivity of U(IV), thereby enhancing its oxidation.

Nanoparticles are considered to be particles measurable on the nanometer scale (Gilbert and Banfield, 2005). Suzuki et al. (2002) reported UO_2 particles as small as 1.5 nm (as estimated by TEM and EXAFS) in U(IV) reducing incubations, which is consistent with UO_2 particle size estimates as small as 0.9 (by EXAFS) and as large as 3 nm (by TEM) that we present here. Nanoparticles may exhibit dramatically different reactive characteristics than their bulk (i.e., measurable on a micrometer or greater scale) counterparts (Hochella, 2002; Gilbert and Banfield, 2005; Hochella and Madden, 2005), and the differences that we have observed in UO_2 reactivity may be due to more complex factors than simply surface area-dependent limits on reactivity. For example, Madden and Hochella (2005) showed that 7.3 nm hematite nanoparticles catalyzed heterogeneous Mn(II) oxidation by O_2 ten times faster than 37 nm particles when normalized for surface area. Similarly, Kucur et al. (2003) showed that variations as small as 0.2 nm in the size of CdSe nanocrystals may have a profound effect on the redox properties of those particles. Therefore, in the nano-size regime, a 2.5 nm UO_2 particle (i.e., $U(IV)_{fast}$ as measured by TEM) could exhibit different redox characteristics than a 3 nm UO_2 particle (i.e., $U(IV)_{slow}$ as measured by TEM), that could not be explained as an exclusively surface area-dependent phenomenon.

Besides the reduction rate-dependent trends in the size of individual UO_2 particles, those particles formed at relatively low rates were also more highly aggregated than those formed at relatively fast rates. In $U(IV)_{slow}$ incubations, we observed UO_2 particles in aggregates of up to 30 nm in diameter. Similarly, Abdelouas et al. (1999) have observed aggregates of UO_2 particles of up to 100 nm. Nanoparticle aggregation is an important step in the formation of larger and more highly ordered phases (Penn and Banfield, 1998; Huang et al., 2003). Huang et al. (2004) showed that aggregation of ZnS nanoparticles induced changes in the bulk structure of the particles, tending toward a more ordered structure with aggregation. Therefore, besides having lower reactive surface area than non-aggregated UO_2 particles, structural changes in UO_2 particles may have been induced upon aggregation, which may have altered their reactivity. We also note here that EXAFS does not allow one to distinguish between an aggregate of nanoparticles and isolated nanoparticles if there is no pseudomorphic orientation of nanoparticles in the aggregate, which underscores the complementary application of TEM and EXAFS in the work presented here and elsewhere (Calvin et al., 2005).

4.3. UO_2 oxidation

Regardless of the oxidant used for U(IV) oxidation, we show here that the size and aggregation state of UO_2 nanoparticles exert strong control on the rate and extent of U(IV) oxidation whether biologic or abiotic. While UO_2

was completely oxidized by oxygen, complete UO_2 oxidation was not observed under any of the anoxic oxidizing conditions tested. Beller (2005) did not observe complete oxidation of UO_2 by *T. denitrificans* under conditions similar to those we used for this work. In the experiments by Beller (2005), only 22% of biogenic UO_2 was oxidized and only 4% of synthetic UO_2 (presumably of larger particle size (Senko et al., 2002; Beyenal et al., 2004)) was oxidized. Beller (2005) also showed more highly aggregated UO_2 particles were less susceptible to nitrate dependent oxidation by *T. denitrificans* (4% disaggregated vs. 0.02% aggregated).

Incomplete oxidation of UO_2 by hydrous ferric oxide (HFO) is a well established phenomenon and may be attributed to the accumulation of Fe(II) and U(VI) products which passivate further reaction between UO_2 and HFO (Senko et al., 2005b; Wan et al., 2005; Ginder-Vogel et al., 2006). The reason for incomplete oxidation of UO_2 by nitrite (with or without Fe as an electron shuttle) is less clear, but may be attributed to thermodynamic (Ginder-Vogel et al., 2006), or physical (e.g., accumulation of U(VI) coatings on UO_2 particle surfaces (Trocellier et al., 1995; Wronkiewicz et al., 1997; Casas et al., 1998)) limitations on the reaction that arise as it proceeds. The susceptibility of biogenic UO_2 to oxidation by nitrite (without Fe as an electron shuttle) is surprising, since nitrite alone has been previously reported to be a relatively ineffective oxidant of U(IV) (Senko et al., 2005b). However, UO_2 used in those previous experiments was autoclaved and treated with 1 M NaOH, which could lead to alterations in the size and surface reactivity of UO_2 particles. The relatively mild treatment (pasteurization) that we subjected biogenic UO_2 particles to in our experiments likely preserved the physical and surface chemical characteristics of the UO_2 particles compared to the relatively harsh conditions used in previous experiments.

Previous work has shown that nitrite may completely oxidize UO_2 when a small amount of Fe is provided to act as an electron shuttle (Senko et al., 2005b), but we did not observe this in the experiments presented here. It is difficult to explain this discrepancy, but the presence of cell material in these experiments (that was not present in the experiments conducted by Senko et al. (2005b)) could play a role in the reactions between U, Fe, and nitrite. While cells were deactivated by pasteurization, remnant biomolecules were included in these incubations, and they may have retained redox activity and other reactive characteristics (e.g., sorption of Fe(II), rendering it unavailable to react with nitrite) after pasteurization. Though remnant cell material was included in the experiments we describe here, a constant cell material concentration was maintained for all experiments, so that we could be assured that the differences in rates and extents of UO_2 oxidation that we observed were not due simply to differences in inactivated biomass concentration.

Understanding the incomplete oxidation of U(IV) in the anoxic incubations is complicated by the observation of two U(IV) species: monomeric U(IV) bound to P and UO_2. It is likely that these species do not reoxidize at the same rate or to the same extent under the conditions tested. Only under conditions where nearly all of the U(IV) is reoxidized can we assume that both species have been transformed from U(IV) to U(VI). Nearly complete oxidation occurred when O_2 was used as an oxidant. These data show that U(IV) resulting from rapid U(VI) bioreduction was oxidized more quickly than that resulting from slow U(VI) bioreduction. The $U(IV)_{fast}$ incubations contained smaller UO_2 particles but also more monomeric U(IV)-P, and it is likely that both of these properties contribute to the faster reoxidation of this sample. Although we can not specifically assign the smaller UO_2 particle size to an increase in reoxidation rate, our data support the conclusion that biogenic U(IV) that is produced at a slow rate is more resistant to reoxidation than that produced at a relatively rapid rate.

In light of the uncertainty regarding the in situ susceptibility of biogenic U(IV) to oxidation and remobilization, recent work has been undertaken to establish conditions that will enhance the stability of biogenic U(IV). The presence of abundant sulfide and/or Fe(II) may prevent oxidative remobilization under oxic conditions by acting as oxygen-scavenging redox buffers (Abdelouas et al., 1999; Zhong et al., 2005). Similarly, abundant reductants may also inhibit the oxidative remobilization of U under nitrate-reducing conditions (Senko et al., 2005b,c; Ginder-Vogel et al., 2006; Moon et al., 2007). Here we show that relatively low rates of U(VI) bioreduction, as manipulated by varying U(VI) reducing bacterial concentration, may give rise to larger and more highly aggregated UO_2 particles that are more resistant to oxidation. It is not clear whether other U(VI) reduction rate-limiting factors (e.g., temperature, U(VI) speciation, other terminal electron acceptors, etc.) would have a similar effect on biogenic UO_2 characteristics. Nevertheless, our results suggest that careful manipulation of in situ U(VI) reduction rates (perhaps by slow addition of electron donor (Fredrickson et al., 2003)) could give rise to UO_2 precipitates in situ that are resistant to oxidative remobilization.

ACKNOWLEDGMENTS

This work was supported by the Environmental Remediation Science Program (ERSP), Office of Biological and Environmental Research (OBER), Office of Energy Research, US Department of Energy (DOE) Grant No. DE-FG02-04ER63914 to The Pennsylvania State University, by the National Science Foundation under Grant No. CHE-0431328 and the US DOE OBER. Support for JMS was also provided by The Pennsylvania State University Center for Environmental Chemistry and Geochemistry. Use of the MR-CAT sector at the Advanced Photon Source (APS) at the Argonne National Laboratory (ANL) was supported by the US DOE, Office of Science, Office of Basic Energy Sciences, under contract W-31-109-ENG-38 and the MRCAT member institutions. Part of this work was performed at the Environmental Molecular Sciences Laboratory (EMSL), a national scientific user facility sponsored by the DOE's OBER, located at the Pacific Northwest National Laboratory (PNNL) in Richland, WA. PNNL is operated for DOE by Battelle Memorial Institute under Contract DE-AC06-76RL0 1830. We thank three reviewers for their valuable input.

APPENDIX A. SUPPLEMENTARY DATA

Supplementary data associated with this article can be found, in the online version, at doi:10.1016/j.gca.2007.07.021.

REFERENCES

Abdelouas A., Lutze W. and Nuttall H. E. (1999) Oxidative dissolution of uraninite precipitated on Navajo sandstone. *J. Contam. Hydrol.* **36**, 353–375.

Anderson R. T., Vrionis H. A., Ortiz-Bernad I., Resch C. T., Long P. E., Dayvault R., Karp K., Marutzky S., Metzler D. R., Peacock A., White D. C., Lowe M. and Lovley D. R. (2003) Stimulating the in situ activity of *Geobacter* species to remove uranium from groundwater of a uranium-contaminated aquifer. *Appl. Environ. Microbiol.* **69**, 5884–5891.

Balch W. E., Fox G. E., Magrum L. J., Woese C. R. and Wolfe R. S. (1979) Methanogens: reevaluation of a unique biological group. *Microbiol. Rev.* **43**, 260–296.

Beller H. R. (2005) Anaerobic, nitrate-dependent oxidation of U(IV) oxide minerals by the chemolithoautotrophic bacterium *Thiobacillus denitrificans*. *Appl. Environ. Microbiol.* **71**, 2170–2174.

Beyenal H., Sani R. K., Peyton B. M., Dohnalkova A. C., Amonette J. E. and Lewandowski Z. (2004) Uranium immobilization by sulfate-reducing biofilms. *Environ. Sci. Technol.* **38**, 2067–2074.

Boyanov M. I., O'Loughlin E. J., Roden E. J., Fein J. B. and Kemner J. M. (2007) Adsorption of Fe(II) and U(VI) to carboxyl-functionalized microspheres: the influence of speciation on uranyl reduction studies by titration and EXAFS. *Geochim. Cosmochim. Acta* **71**, 1898–1912.

Brina R. and Miller A. G. (1992) Direct detection of trace levels of uranium by laser-induced kinetic phosphorimetry. *Anal. Chem.* **64**, 1413–1428.

Burgos W. D., Senko J. M., Dempsey B. A., Roden E. E., Kemner K. M. and Kelly S. D. (2007) Soil humic acid decreases biological uranium(VI) reduction by *Shewanella putrefaciens* CN32. *Environ. Eng. Sci.* **24**, 200–206.

Burns P. C. (1999) The crystal chemistry of uranium. *Rev. Mineral.* **38**, 23–90.

Calvin S., Luo S. X., Caragianis-Broadbridge C., McGuiness J. K., Anderson E., Lehman A., Wee K. H., Morrison S. A. and Kurihara L. K. (2005) Comparison of extended X-ray absorbtion fine structure and Scherrer analysis of X-ray diffraction as methods for determining mean sizes of polydisperse nanoparticles. *Appl. Phys. Lett.* **87**, 233102-1-3.

Casas I., de Pablo J., Giménez J., Torrero M. E., Bruno J., Cera E., Finch R. J. and Ewing R. C. (1998) The role of pe, pH, and carbonate on the solubility of UO_2 and uraninite under nominally reducing conditions. *Geochim. Cosmochim. Acta* **62**, 2223–2231.

Cornell R. M. and Schwertmann U. (2003) The Iron Oxides, second ed. Wiley-VCH, Weinheim, Germany.

DiSpirito A. A. and Tuovinen O. H. (1982) Uranous ion oxidation and carbon dioxide fixation by *Thiobacillus ferrooxidans*. *Arch. Microbiol.* **133**, 28–32.

Deng Y. and Stumm W. (1994) Reactivity of aquatic iron(III)oxyhydroxides-implications for redox cycling of iron in natural waters. *Appl. Geochem.* **9**, 23–36.

Duff M. C., Hunter D. B., Bertsch P. M. and Amrhein C. (1999) Factors influencing uranium reduction and solubility in evaporation pond sediments. *Biogeochemistry* **45**, 95–114.

Elias D. E., Senko J. M. and Krumholz L. R. (2003) A procedure for the quantitation of total oxidized uranium for bioremediation studies. *J. Microbiol. Meth.* **53**, 343–353.

Finneran K. T., Housewright M. E. and Lovley D. R. (2002) Multiple influences of nitrate on uranium solubility during bioremediation of uranium-contaminated subsurface sediments. *Environ. Microbiol.* **4**, 510–516.

Francis A. J., Gillow J. B., Dodge C. J., Harris R., Beveridge T. J. and Papenguth H. W. (2004) Uranium association with halophilic and non-halophilic bacteria and archaea. *Radiochim. Acta* **92**, 481–488.

Fredrickson J. K., Zachara J. M., Kennedy D. W., Liu C. G., Duff M. C., Hunter D. B. and Dohnalkova A. (2002) Influence of Mn oxides on the reduction of uranium by the metal-reducing bacterium *Shewanella putrefaciens*. *Geochim. Cosmochim. Acta* **66**, 3247–3262.

Fredrickson J. K., Kota S., Kukkadapu R. K., Liu C. and Zachara J. M. (2003) Influence of electron donor/acceptor concentrations on hydrous ferric oxide (HFO) bioreduction. *Biodegradation* **14**, 91–103.

Gilbert B. and Banfield J. F. (2005) Molecular-scale processes involving nanoparticulate minerals in biogeochemical systems. *Rev. Mineral.* **59**, 109–155.

Ginder-Vogel M., Criddle C. S. and Fendorf S. (2006) Thermodynamic constraints on the oxidation of biogenic UO_2 by Fe(III) (hydr)oxides. *Environ. Sci. Technol.* **40**, 3544–3550.

Glasauer S., Weidler P. G., Langley S. and Beveridge T. J. (2003) Controls on Fe reduction and mineral formation by a subsurface bacterium. *Geochim. Cosmochim. Acta* **67**, 1277–1288.

Gorby Y. A. and Lovley D. R. (1992) Enzymic uranium precipitation. *Environ. Sci. Technol.* **26**, 205–207.

Gorby Y. A., Yanina S., McLean J. S., Rosso K. M., Moyles D., Dohnalkova A., Beveridge T. J., Chang I. S., Kim B. H., Kim K. S., Culley D. E., Reed S. B., Romine M. F., Saffarini D. A., Hill E. A., Shi L., Elias D. A., Kennedy D. W., Pinchuk G., Watanabe K., Ishii S., Logan B., Nealson K. H. and Fredrickson J. K. (2006) Electrically conductive bacterial nanowires produced by *Shewanella oneidensis* strain MR-1 and other organisms. *Proc. Nat. Acad. Sci. USA* **103**, 11358–11363.

Han Y. S., Hadiko G., Fuji M. and Takahashi M. (2005) Effect of flow rate and CO_2 content on the phase and morphology of $CaCO_3$ prepared by bubbling method. *J. Cryst. Growth* **276**, 541–548.

Hansel C. M., Benner S. G., Nico P. and Fendorf S. (2004) Structural constraints of ferric (hydr)oxides on dissimilatory iron reduction and the fate of Fe(II). *Geochim. Cosmochim. Acta.* **68**, 3217–3329.

Hochella, Jr., M. F. (2002) Nanoscience and technology: the next revolution in the Earth sciences. *Earth Planet. Sci. Lett.* **203**, 593–605.

Hochella, Jr., M. F. and Madden A. S. (2005) Earth's nanocompartments for toxic metals. *Elements* **1**, 199–203.

Huang F., Zhang H. and Banfield J. F. (2003) Two-stage crystal-growth kinetics observed during hydrothermal coarsening of nanocrystalline ZnS. *Nano Lett.* **3**, 373–378.

Huang F., Gilbert B., Zhang H. and Banfield J. F. (2004) Reversible, surface-controlled structure transformation in nanoparticles induced by an aggregation state. *Phys. Rev. Lett.* **92**, 155501-1–15501-4.

Istok J. D., Senko J. M., Krumholz L. R., Watson D., Bogle M.-A., Peacock A. D., Chang Y.-J. and White D. C. (2004) In situ bioreduction of technetium and uranium in a nitrate contaminated aquifer. *Environ. Sci. Technol.* **38**, 468–475.

Kelly S. D., Kemner K. M., Fein J. B., Fowle D. A., Boyanov M. I., Bunker B. A. and Yee N. (2002) X-ray absorption fine structure determination of pH-dependent U-bacterial cell wall interactions. *Geochim. Cosmochim. Acta* **66**, 3855–3871.

Kemner K. M., Kelly S. D., Lai L., Maser J., O'Loughlin E. J., Sholto-Douglas D., Cai Z., Schneegurt M. A., Kulpa, Jr., C. F. and Nealson K. H. (2004) Elemental and redox analysis of single bacterial cells by X-ray microbeam analysis. *Science* **306**, 686–687.

Kucur E., Riegler J., Urban G. A. and Nann T. (2003) Determination of quantum confinement in CdSe nanocrystals by cyclic voltammetry. *J. Chem. Phys.* **119**, 2333–2337.

Liger E., Charlet L. and Van Cappellen P. (1999) Surface catalysis of uranium(VI) reduction by iron(II). *Geochim. Cosmochim. Acta* **63**, 2939–2955.

Locock A. J. and Burns P. C. (2003) The crystal structure of synthetic autunite, $Ca[(UO_2)(PO_4)]_2(H_2O)_{11}$. *Am. Mineral.* **88**, 240–244.

Lovley D. R. and Phillips E. J. P. (1987) Rapid assay for microbially reducible ferric iron in aquatic sediments. *Appl. Environ. Microbiol.* **53**, 1536–1540.

Lovley D. R., Phillips E. J. P., Gorby Y. A. and Landa E. R. (1991) Microbial reduction of uranium. *Nature* **350**, 413–416.

Madden A. S. and Hochella, Jr., M. F. (2005) A test of geochemical reactivity as a function of mineral size: manganese oxidation promoted by hematite nanoparticles. *Geochim. Cosmochim. Acta* **69**, 389–398.

Marshall M. J., Beliaev A. S., Dohnalkova A. C., Kennedy D. W., Shi L., Wang S., Boyanov M. I., Lai B., Kemner K. M., McLean J. S., Reed S. B., Culley D. E., Bailey V. L., Simonson C. J., Saffarini D. A., Romine M. F., Zachara J. M. and Fredrickson J. K. (2006) *c*-type cytochrome-dependent formation of U(IV) nanoparticles by *Shewanella oneidensis*. *PLoS Biol.* **4**, 1324–1333.

McDonough, J.M. (2006) Kinetics of Biological Uranium(VI) Reduction and Subsequent Uranium (IV) Oxidation. MS Thesis, The Pennsylvania State University, University Park, PA.

Moon H. S., Komlos J. and Jaffé P. R. (2007) Uranium reoxidation in previously bioreduced sediment by dissolved oxygen and nitrate. *Environ. Sci. Technol.* **41**, 4587–4592.

Morosin B. (1978) Hydrogen uranyl phosphate tetrahydrate, a hydrogen ion solid electrolyte. *Acta Crystallogr. B* **34**, 3732–3734.

Murphy W. M. and Shock E. L. (1999) Environmental aqueous geochemistry of actinides. *Rev. Mineral.* **38**, 221–253.

Nevin K. P. and Lovley D. R. (2000) Potential for nonenzymatic reduction of Fe(III) via electron shuttling in subsurface sediments. *Environ. Sci. Technol.* **34**, 2472–2478.

Newville M. (2001) IFEFFIT: interactive EXAFS analysis and FEFF fitting. *J. Synch. Rad.* **8**, 322–324.

Newville M., Livins P., Yacoby Y., Rehr J. J. and Stern E. A. (1993) Near-edge X-ray absorption fine structure of Pb: a comparison of theory and experiment. *Phys. Rev. B* **14**, 14126–14131.

O'Loughlin E. J., Kelly S. D., Cook R. E., Csencsits R. and Kemner K. M. (2003) Reduction of uranium(IV) by mixed iron(II)/iron(III) hydroxide (green rust): formation of UO_2 nanoparticles. *Environ. Sci. Technol.* **37**, 721–727.

Parsons T. R., Maita Y. and Lalli C. M. (1984) Direct counting of bacteria by fluorescence microscopy. In *A Manual of Chemical and Biological Methods for Seawater Analysis*. Pergamon Press, New York, pp. 123–126.

Penn R. L. and Banfield J. F. (1998) Imperfect oriented attachment: dislocation generation in defect-free nanocrystals. *Science* **281**, 969–971.

Pierce E. M., Icenhower J. P., Serne R. J. and Catalano J. G. (2005) Experimental determination of $UO_{2(cr)}$ dissolution kinetics: effects of solution saturation state and pH. *J. Nucl. Mater.* **345**, 206–218.

Ravel B. and Newville M. (2005) ATHENA, ARTEMIS, HEPHAESTUS: data analysis for X-ray absorption spectroscopy using IFEFFIT. *J. Synch. Rad.* **12**, 537–541.

Roden E. E. (2003) Fe(III) oxide reactivity toward biological versus chemical reduction. *Environ. Sci. Technol.* **37**, 1319–1324.

Schwertmann U. and Cornell R. M. (1991) Iron Oxides in the Laboratory. Wiley, New York.

Segre, C.W., Leyarovska, N.E., Chapman, L.D., Lavender, W.M., Plag, P.W., King, A.S., Kropf, A.J., Bunker, B.A., Kemner, K.M., Dutta, P., Druan, R.S., Kaduk, J. (2000) Synchrotron Radiation Instrumentation: Eleventh U. S. Conference. American Institute of Physics, College Park, MD. pp. 419–422.

Senko J. M., Istok J. D., Suflita J. M. and Krumholz L. R. (2002) In situ evidence for uranium immobilization and remobilization. *Environ. Sci. Technol.* **36**, 1491–1496.

Senko J. M., Dewers T. A. and Krumholz L. R. (2005a) Effect of oxidation rate and Fe(II) state on microbial nitrate-dependent Fe(III) mineral formation. *Appl. Environ. Microbiol.* **71**, 7172–7177.

Senko J. M., Mohamed Y., Dewers T. A. and Krumholz L. R. (2005b) Role for Fe(III) minerals in nitrate-dependent microbial U(IV) oxidation. *Environ. Sci. Technol.* **39**, 2529–2536.

Senko J. M., Suflita J. M. and Krumholz L. R. (2005c) Geochemical controls on microbial nitrate-dependent U(IV) oxidation. *Geomicrobiol. J.* **22**, 317–378.

Stern E. A., Newville M., Ravel B., Yacoby Y. and Haskel D. (1995) The UWXAFS analysis package – philosophy and details. *Physica B* **209**, 117–120.

Suzuki Y., Kelly S. D., Kemner K. M. and Banfield J. F. (2002) Radionuclide contamination -nanometre-size products of uranium bioreduction. *Nature* **419**, 134.

Suzuki Y., Kelly S. D., Kemner K. M. and Banfield J. F. (2003) Enzymatic U(VI) reduction by *Desulfosporosinus* species. *Radiochim. Acta* **92**, 11–16.

Tanner R. S. (1997) Cultivation of bacteria and fungi. In *Manual of Environmental Microbiology* (eds. C. J. Hurst, G. R. Knudsen, M. J. McInerney, L. D. Stetzenbach and M. V. Walter). American Society for Microbiology, Washington, DC, pp. 52–59.

Trocellier P., Gallien J. P. and Cachoir C. (1995) Study of the leaching behaviour of sintered UO_2 in groundwater using nuclear microprobe techniques. *Mater. Res. Soc. Proc.* **353**, 585–592.

van der Zee C., Roberts D. R., Rancourt D. G. and Slomp C. P. (2003) Nanogoethite is the dominant reactive oxyhydroxide phase in lake and marine sediments. *Geology* **31**, 993–996.

Wan J., Tokunaga T. K., Brodie E., Wang Z., Zheng Z., Herman D., Hazen T., Firestone M. K. and Sutton S. R. (2005) Reoxidation of bioreduced uranium under reducing conditions. *Environ. Sci. Technol.* **39**, 6162–6169.

Wersin P., Hochella, Jr., M. F., Persson P., Redden G., Leckie J. O. and Harris D. W. (1994) Interaction between aqueous uranium(VI) and sulfide minerals: spectroscopic evidence for sorption and reduction. *Geochim. Cosmochim. Acta* **58**, 2829–2843.

Wronkiewicz D. J., Buck E. C. and Bates J. K. (1997) Grain boundary corrosion and alteration phase formation during the oxidative dissolution of UO_2 pellets. *Mat. Res. Soc. Symp. Proc.* **465**, 519–526.

Wyckoff R. W. G. (1960). *Crystal Structures.* vol. 1. Interscience Publishers, New York.

Zabinski S. I., Rehr J. J., Ankudinov A., Albers R. C. and Eller M. J. (1995) Multiple-scattering calculations of X-ray-absorption spectra. *Phys. Rev. B* **52**, 2995–3009.

Zachara J. M., Fredrickson J. K., Li S.-M., Kennedy D. W., Smith S. C. and Gassman P. L. (1998) Bacterial reduction of crystalline Fe^{3+} oxides in single phase suspensions and subsurface materials. *Am. Mineral.* **83**, 1426–1443.

Zhong L., Liu C., Zachara J. M., Kennedy D. W., Szecsody J. E. and Wood B. (2005) Oxidative remobilization of biogenic uranium(IV) precipitates: effects of iron(II) and pH. *J. Environ. Qual.* **34**, 1763–1771.

Associate editor: Jack J. Middleburg